Microstructure characterisation and mechanical properties of ODS Eurofer steel subject to designed heat treatments

Fu, J.; Brouwer, J. C.; Hendrikx, R. W.A.; Richardson, I. M.; Hermans, M. J.M.

DOI
10.1016/j.msea.2019.138568

Publication date
2020

Document Version
Final published version

Published in
Materials Science and Engineering A

Materials Science & Engineering A 770 (2020) 138568

Contents lists available at ScienceDirect

Materials Science & Engineering A

journal homepage: http://www.elsevier.com/locate/msea

Microstructure characterisation and mechanical properties of ODS Eurofer steel subject to designed heat treatments

J. Fu [a,b,*], J.C. Brouwer [a], R.W.A. Hendrikx [a], I.M. Richardson [a], M.J.M. Hermans [a]

[a] Department of Materials Science and Engineering, Delft University of Technology, Delft, the Netherlands
[b] Dutch Institute for Fundamental Energy Research (DIFFER), the Netherlands

ARTICLE INFO

Keywords:
Oxide dispersion strengthened steels
Powder metallurgy
Heat treatment
Microstructure
Yield strength modelling

ABSTRACT

The present work deals with oxide dispersion strengthened (ODS) Eurofer steel fabricated by powder metallurgy involving mechanical alloying and spark plasma sintering. A heat treatment route including normalising and tempering was applied to the as-produced steel, based on differential scanning calorimetry (DSC) measurement. The microstructure was characterised by scanning electron microscopy (SEM), electron backscattered diffraction (EBSD), electrolytic extraction, X-ray diffraction (XRD) and transmission electron microscopy (TEM). Thermodynamic calculations conducted using Thermo-Calc software were used to determine the precipitation conditions. The results show that the Vickers microhardness of the sample after the designed heat treatment is more uniform compared to the as-produced condition. A dual phase and bimodal microstructure is formed in the as-produced and tempered steels. $M_{23}C_6$ and M_6C carbides were found in the as-produced sample while only $M_{23}C_6$ carbides were observed in the tempered sample. The carbides dissolve and reprecipitate during the heat treatment, preferably at the grain boundaries. Nanosized Y_2O_3 particles were found to be homogenously distributed in the steel matrix, which is crucial for the mechanical properties. The dislocation density in the material is decreased significantly after the normalising and tempering treatment. A yield strength model was developed that includes the strengthening contributions of solid solutes, grain size, dislocation density and nanoparticles. Good agreement is obtained between the experimentally measured and theoretically calculated strength of the as-produced and tempered steels.

1. Introduction

Nano-structured oxide dispersion strengthened (ODS) steels are candidate cladding materials for advanced nuclear fission and fusion applications due to an excellent creep strength at high temperature and low swelling under irradiation [1–3]. The superior performance of ODS steels in comparison with the conventional ferritic steels is attributed to the high number density of nano-sized oxide particles. The interface between the matrix and nano-oxides can act as trap sites for He atoms preventing the formation of large voids, and as a stable sink for irradiation induced primary defects, such as vacancies and interstitial atoms [1].

The addition of nano-oxides into the steel matrix is typically accomplished by mechanical alloying (MA), in which metastable solid solutions and nano-particle dispersions are formed [4]. The mechanically alloyed powders are then consolidated at high temperature and pressure, usually through hot extrusion (HE) or hot isostatic pressing (HIP), to produce the bulk steel. However, these processes require relatively long processing times at high temperatures that may cause grain growth and precipitate coarsening [5]. Spark plasma sintering (SPS) is a novel consolidation technique utilizing uniaxial force and a pulsed direct electrical current to perform high speed consolidation of the powder. SPS has many advantages over HE and HIP including: a lower sintering temperature, higher heating rates, shorter holding times, and accurate control over each stage of the sintering process, all of which contribute to maintaining the intrinsic properties of nanopowders in near full densification with minimum grain growth [6,7].

SPS allows fabrication of bulk materials through rapid densification. However, the short duration of the deformation process will cause a significant change of properties and an increased number of defects in the material, leading to a metastable microstructure [8]. Meanwhile, after the SPS process, the cooling of the ODS steels in the mould is relatively slow, leading to coarsening of the prior austenite grains and a partial martensite transformation, which will probably cause the

* Corresponding author.
E-mail address: j.fu@tudelft.nl (J. Fu).

https://doi.org/10.1016/j.msea.2019.138568
Received 3 June 2019; Received in revised form 5 September 2019; Accepted 15 October 2019
Available online 16 October 2019

degradation of the mechanical properties [9]. Therefore, a post heat treatment is usually applied after SPS to recover the initial microstructure and improve the mechanical performance [10,11].

This study is a continuation of our previous work [12], where MA and SPS were successfully employed to produce high performance ODS Eurofer steel, based on the European reduced-activation ferritic martensitic reference steel Eurofer 97. Despite the large number of published results, there is still a lack of systematic study on the heat treatment effects on the microstructure and mechanical properties of MA and SPS produced ODS Eurofer. For this purpose, a post heat treatment route was designed based on the results of differential scanning calorimetry (DSC) and Vickers microhardness measurements. The microstructural features were studied by means of scanning electron microscopy (SEM), electron backscattered diffraction (EBSD), X-Ray diffraction (XRD) and transmission electron microscopy (TEM). The dislocation densities of the as-produced and heat-treated steels were determined by XRD. Finally, a yield strength model was proposed to evaluate the contributions of solute atoms, grain size, dislocation density and nanosized particles.

2. Experimental details

2.1. Materials

Blended high purity elemental powders with a chemical composition of Fe–9Cr–1.1W–0.4Mn–0.2V–0.12Ta–0.3Y_2O_3 (wt%), provided by Goodfellow, Germany and Alfa Aesar, Germany, were used for the production of ODS Eurofer steel. The powders were mechanical alloyed in an Ar atmosphere for 30 h at 300 rpm with a ball to powder mass ratio of 3.4:1 in a Retsch planetary ball milling machine. Powders were then sintered in a Spark Plasma Sintering machine (SPS, FCT group, Germany) at 1100 °C with a heating rate of 100 °C/min. A pressure of 60 MPa was applied throughout the SPS process. Disks of 40 mm diameter and 10 mm thickness were produced after a holding time of 30 min. These parameters were selected based on our previous study [12]. The chemical composition of the as-produced steel, obtained through X-Ray Fluorescence (for heavy elements) and combustion analysis (for carbon), is listed in Table 1.

2.2. Methods

Thermal analysis of the as-produced ODS Eurofer was conducted by means of differential scanning calorimeter (DSC) to obtain the DSC profile. The test was operated in an argon atmosphere with a flow rate of 100 ml/min. A well cleaned sample with a mass of around 63 mg was used. The applied thermal cycle was designed as follows: the specimen was heated to 1250 °C at a heating rate of 10 °C/min and held at this temperature for 10 min, and then cooled to room temperature at a cooling rate of 10 °C/min. The base line determination and subtraction were performed by using an empty crucible with identical heating and cooling rates.

A heat treatment route was applied to the as-produced steel to restore ductility and improve the performance. The steel was subject to a normalisation treatment for 1 h at 1050 °C, 1150 °C and 1250 °C, respectively. In the case of a normalisation treatment at 1150 °C, a tempering treatment was followed at 600 °C, 700 °C and 800 °C for 1 h, respectively. All specimens were air cooled to room temperature. Vickers microhardness was measured from the top surface to the bottom surface of the samples, with a load of 0.3 kg and a step size of 0.5 mm.

The microstructure was investigated using a JEOL 6500F scanning electron microscope (SEM) with an electron backscattered diffraction (EBSD) and a JEM-2200FS transmission electron microscope (TEM) equipped with an energy dispersive spectrometer (EDS) system. To reveal the microstructure for SEM observations, the samples were etched in a mixed solution of 5 g ferric chloride, 50 ml HCl and 100 ml water for 20 s. Specimens for EBSD were mirror polished followed by an alumina suspension polishing step. The TEM specimens were prepared by electropolishing disks with a diameter of 3 mm in a twin-jet electropolisher using 10% perchloric acid and 90% ethanol as electrolyte. For characterisation of carbides in the steel, precipitates were electrolytically extracted using a solution of 10% hydrochloric acid, 1% citric acid, balance ethanol, with a current density of 0.1 A/cm^2 at room temperature. The residues were separated using a centrifuge rotating at 18 000 rpm for 3 min. The extracted residues were then analysed by X-Ray diffraction (XRD) with Cu Kα target ($\lambda = 1.5406$ Å, 45 kV and 40 mA). A step size of 0.03° and a measuring time of 2 s per step were employed. LaB6 powder was used for the determination of the instrumental contributions to the peak width. To elucidate the mechanism of the formation of carbides precisely, computation of the phase diagram of ODS Eurofer was performed, using the Thermo-Calc code and TCFE6 database. The dislocation density of the material was calculated using XRD, with the same parameters stated above.

3. Results and discussion

3.1. Design of heat treatment route

The DSC profile of the as-produced steel obtained during heating and cooling processes can be seen in Fig. 1. In the heating stage, two distinct endothermic peaks are identified. The first one is caused by the Curie transition and the second is related to the ferrite to austenite transformation. The starting temperature (Ac1) and finishing temperature (Ac3) of the austenite transformation are determined as 822.9 °C and 869.4 °C, respectively. A peak corresponding to the δ-ferrite transformation can be seen around 1200 °C. In the cooling stage, two exothermic peaks can be observed, which are associated with the Curie transition and the martensite transformation, respectively. The change of the heat flow of the second peak is small, probably because the cooling rate is not high enough to achieve a full martensitic

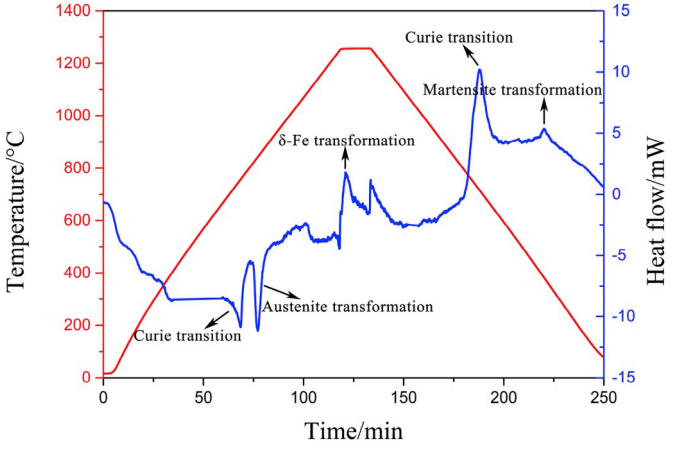

Fig. 1. DSC profile of the as-produced steel obtained during heating and cooling schedule.

Table 1
Chemical composition of the bulk steel in wt%.

	Cr	W	Mn	V	Ta	Y	Al	C	Fe
As-produced steel (wt%)	8.92	0.99	0.45	0.20	0.15	0.21	0.09	0.09	Bal.

transformation. The starting temperature (M_s) and finishing temperature (M_f) of martensite transformation are 387.5 °C and 339.1 °C, respectively.

In order to obtain a recovered microstructure as well as relatively uniform mechanical properties of the material, a two-step heat treatment route including normalising and tempering treatment was designed. The main goal of normalising treatment is to enhance the mechanical properties of the material by refining the microstructure, which is realised by the solid state phase transformation. The normalising temperature should be higher than Ac3. Moreover, according to the study of normalising treatment on ODS Eurofer by Lu et al. [13], the normalising temperature should be lower than 1300 °C to avoid coarsening of the microstructure; therefore, three normalising temperatures were chosen: 1050 °C, 1150 °C and 1250 °C. As the steel is air cooled after normalising, (part of) the microstructure is transformed to a brittle martensite with higher dislocation density. To relieve the normalising stress and achieve a desired balance of mechanical properties, a high temperature tempering step should be applied [14]. The tempering temperature should be below Ac1 to avoid the formation of fresh martensite, which otherwise would cause a decrease in the material toughness [15]. Tempering temperatures were chosen to be 600 °C, 700 °C and 800 °C.

Fig. 2 shows a Vickers hardness profile of the cross section of the as-produced and heat-treated samples. It can be seen that there is a large variation in the hardness profile of the as-produced sample. The top and bottom surfaces have a higher hardness of approximately 650 HV whereas the middle area has a lower hardness of approximately 400 HV. This is probably due to a larger number of carbides and a more rapidly cooling in the surface area according to our previous study [12]. After a heat treatment at 1050 °C for 1 h, the hardness of the material does not change significantly. This could be ascribed to a competitive effect of grain growth and martensite transformation in this condition. After a normalising treatment at 1150 °C and 1250 °C for 1 h, the hardness of the materials are increased remarkably, indicating the occurrence of martensite transformation. It is worth mentioning that part of the material was detached from the base metal after normalising at 1250 °C. Therefore, 1150 °C was selected as a more appropriate normalising temperature. Upon tempering, defect recovery, carbon diffusion and carbide precipitation will usually occur in dual phase steels [14]. It can be seen that after tempering at 600 °C for 1 h, the difference of the hardness in the material has been partially eliminated. After tempering at 700 °C and 800 °C for 1 h, the average hardness of the samples are 348.1 ± 17.7 and 334.6 ± 20.4 HV, respectively. A more homogenous microstructure and mechanical properties compared to the as-produced material are obtained. The hardness of the sample tempered at 800 °C is slightly lower than the one tempered at 700 °C, probably due to carbide coarsening and grain growth, which will affect the strength of the material. The condition of normalising at 1150 °C and tempering at 700 °C was therefore determined as a more suitable heat treatment route. The microstructure and mechanical properties of the steel subject to this condition were investigated and the steel is referred to as "tempered steel".

Fig. 3 shows the EBSD maps of ODS Eurofer under different conditions, with grain colours related to grain orientation expressed in the standard triangle. TSL OIM analysis software was used to determine the grain size. The effective grain boundaries were chosen as the high angle grain boundaries with misorientations larger than 15°. It can be seen from Fig. 3a that the microstructure of as-produced ODS Eurofer consists of coarse grains and fine grains. From the results of the software, the grain size distribution is bimodal, with peaks at 0.29 and 4.72 μm. Finer grains smaller than 0.29 μm could not be indexed, causing the non-indexed (black) areas in the figure. Similar bimodal grain size distributions have been widely reported for powder metallurgy prepared ODS steels. This microstructure could result from heterogenous recrystallization due to an inhomogenous dislocation density after the milling process [16–18], combined with a spatial variation in the pinning force by a nonuniform distribution of nanoparticles [17–19]. More importantly, materials with a bimodal microstructure have proven to have a good compromise between strength and ductility [20,21]. In these materials, ultrafine grains induce high strength as expected from an extrapolation of the Hall-Petch relationship, while the coarse grains provide substantial strain-hardening, therefore ensure retained ductility [22].

Fig. 4 shows the average grain size obtained from the EBSD data for the different conditions in Fig. 3. It can be seen that with the increase of normalising temperature, the average grain size slightly decreases. This phenomenon could be ascribed to a competition between martensite transformation and grain growth due to the increase of normalising temperature (according to the result of the TSL OIM software, the average grain size of martensite is smaller than ferrite). Moreover, according to the studies of Zilnyk et al. [23] and Lu et al. [13], there is a significant increase in the grain size of Eurofer 97 after a normalising treatment above 1000 °C for 1 h. This confirms that the pinning effect on the grain boundaries by Y_2O_3 nanoparticles is very effective even at these high temperatures. Grain growth occurs after normalising and tempering treatment (Fig. 4e), due to a lack of martensite transformation during the tempering process.

3.2. Microstructure characterisation

The optical micrographs of the as-produced and tempered steel can be seen in Fig. 5. Martensite (dark regions) and residual ferrite (white

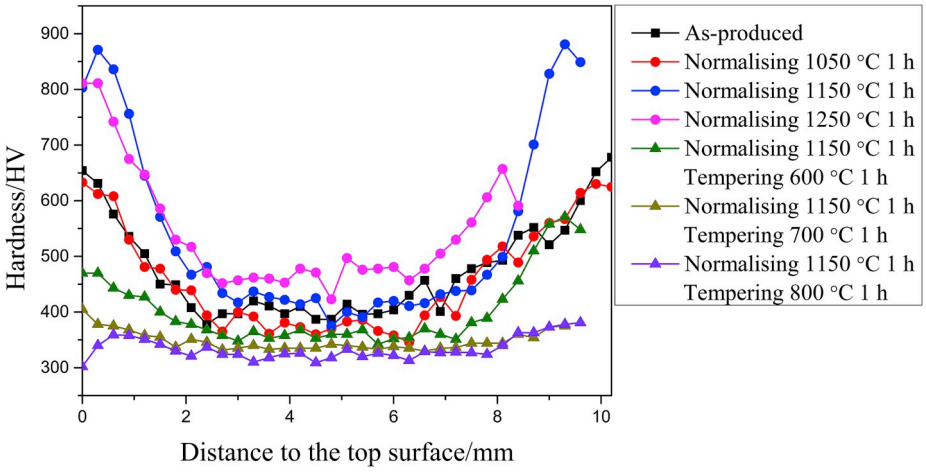

Fig. 2. Vickers hardness profile of the cross section of the as-produced and heat-treated samples.

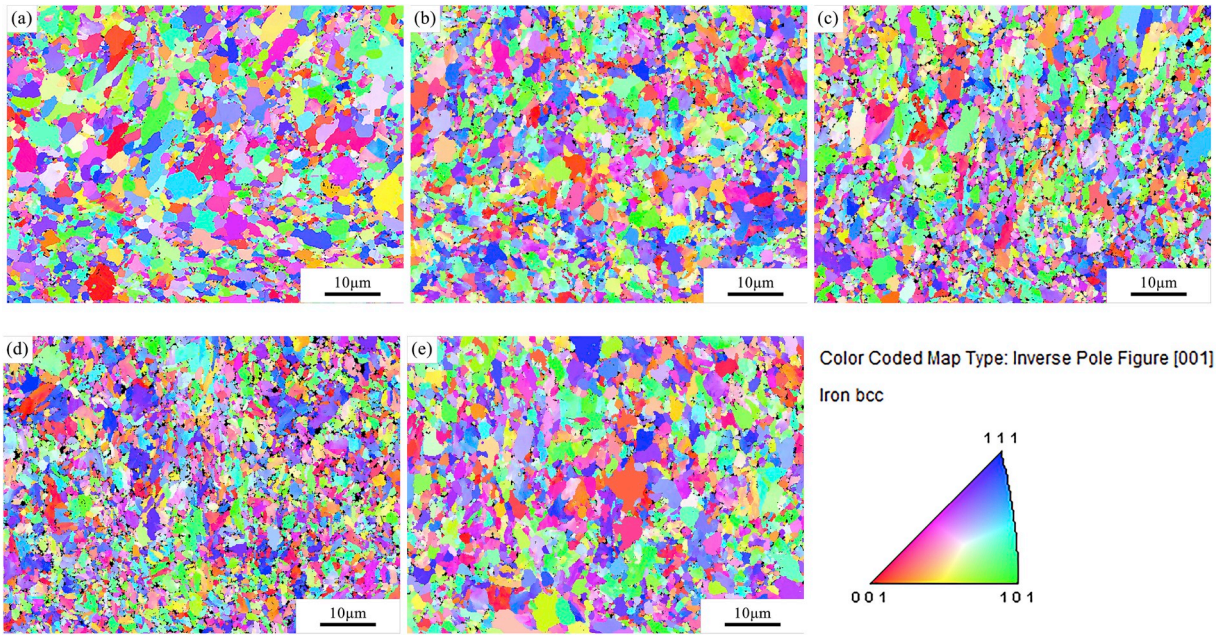

Fig. 3. EBSD maps of ODS Eurofer at different conditions: (a) as-produced, (b) Normalising at 1050 °C, (c) Normalising at 1150 °C, (d) Normalising at 1250 °C and (e) Normalising at 1150 °C tempering at 700 °C.

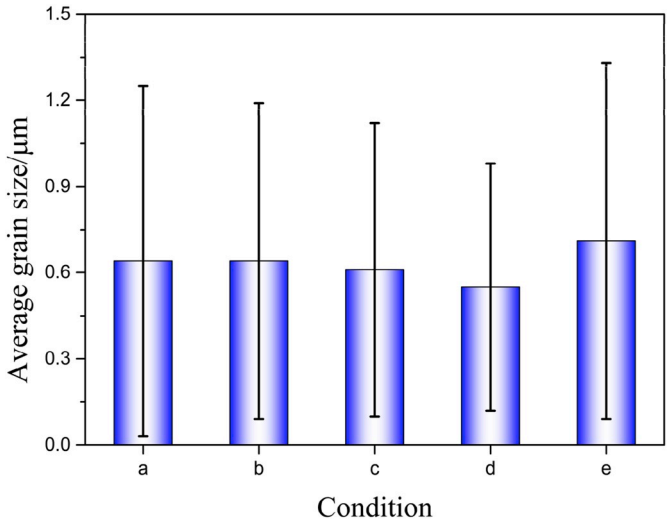

Fig. 4. Average grain size obtained from EBSD data for different conditions in Fig. 3: (a) as-produced, (b) Normalising at 1050 °C, (c) Normalising at 1150 °C, (d) Normalising at 1250 °C and (e) Normalising at 1150 °C tempering at 700 °C.

regions) are revealed in both conditions. The as-produced steel having a martensitic microstructure is probably due to the sintering temperature (1100 °C) above Ac1, hence martensite is formed during the cooling process. The formation of residual ferrite in Fig. 5b is unusual, as after a normalising treatment, a fully martensitic microstructure is expected to form. Yamamoto et al. [24] and Cayron et al. [25] also reported the presence the residual ferrite after a normalising treatment of ODS Fe–9Cr steels. This phenomenon may be because the austenite transformation is partly suppressed in the material, as the ferrite–austenite interface motion is strongly pinned by finely dispersed oxide particles during the heat treatment.

The SEM micrographs of the as-produced and tempered steel are shown in Fig. 6. Precipitates rich in Fe, Cr and C are confirmed by energy dispersive spectrometer (EDS). Based on the average particle size and chemical composition, they are assumed to be Fe–Cr carbides. It is worth noting that after the heat treatment, the carbides are more preferentially located on the grain boundaries. The carbides dissolve and reprecipitate during the normalising and tempering treatment, and Fe–Cr carbides tend to precipitate along the prior austenite grain boundaries due to a decrease in volume free energy [26]. The presence of Fe–Cr carbides is beneficial for the mechanical strength, as they are effective in inhibiting the motion of grain boundaries, acting as obstacles to block the dislocation motion and subgrain formation [27].

In order to characterise the carbides more precisely, the particles

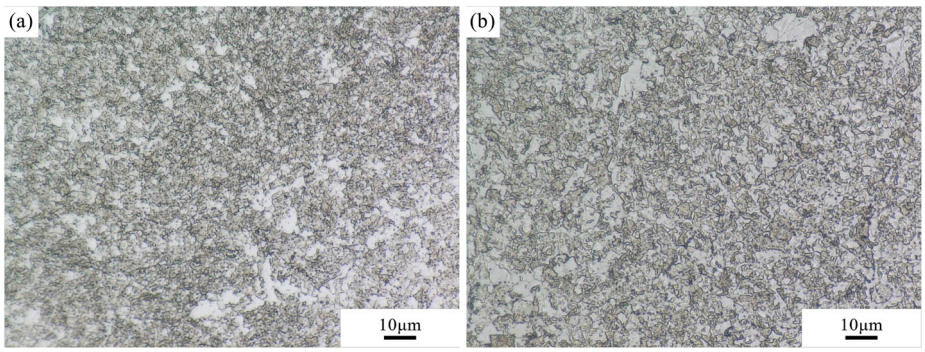

Fig. 5. Optical micrographs of the (a) as-produced and (b) tempered steel.

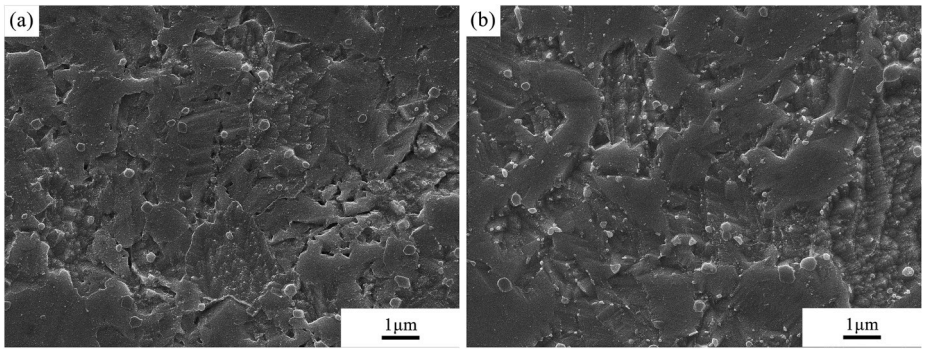

Fig. 6. SEM micrographs of the (a) as-produced and (b) tempered steel.

were electrolytically extracted and analysed by XRD, as shown in Fig. 7. The presence of $(Fe_3W_3)C$, referred to as M_6C and $(Cr_{15.58}Fe_{7.24})C_6$, referred to as $M_{23}C_6$ were confirmed in the as-produced steel, while only $M_{23}C_6$ carbides were observed in the tempered steel. The measured lattice constants obtained from different 2θ values were plotted as a function of $cos2(\theta)/sin(\theta) + cos2(\theta)/\theta$, the Nelson-Riley function, and extrapolated to $\theta = 90°$ to minimise absorption errors [28]. After calculation, the lattice constants of the M_6C and $M_{23}C_6$ carbides in the as-produced sample are determined as 11.081 Å and 10.577 Å, respectively; the lattice constant of the $M_{23}C_6$ carbides in the tempered sample is 10.616 Å.

The phase diagram of ODS Eurofer with respect to the carbon content was calculated using Thermo-Calc software and is shown in Fig. 8. The computations were performed using a defined composition of Fe–9Cr–1.1W–0.4Mn–0.2V–0.12Ta–0.3Y_2O_3 (wt%). The dash line indicates a carbon content of 0.09%, corresponding to the chemical composition shown in Table 1. The starting temperature of the austenite transformation predicted by the phase diagram is 826.8 °C, very close to that obtained by the DSC measurement (822.9 °C). At room temperature, for a carbon content of more than 0.07%, $M_{23}C_6$ carbides would form in the α-Fe matrix, whereas M_6C carbides are predicted to form at a carbon content of less than 0.07%. The formation of carbides is probably due to the carbon diffusion from the graphite mould during the SPS process, as no carbon powder was added to the precursor powder for mechanical alloying. As the SPS was conducted at a maximum temperature of 1100 °C, the carbon can diffuse into the sample to some extent. The diffusion results in an inhomogeneous distribution of carbon in the bulk steel. Higher carbon levels are formed near the surface area and less

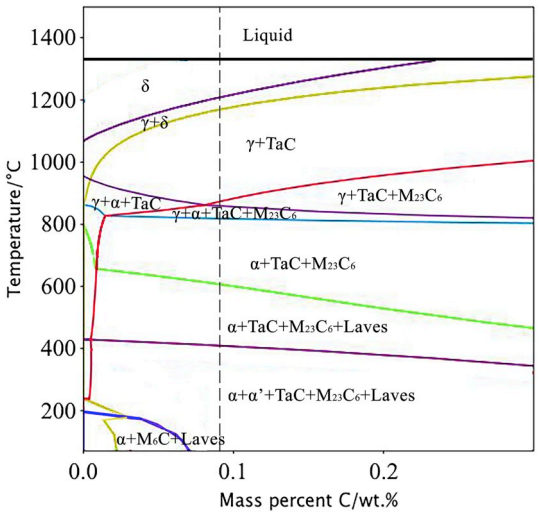

Fig. 8. Computed phase diagram with respect to the carbon content for Fe–9Cr–1.1W–0.4Mn–0.2V–0.12Ta–0.3Y_2O_3 (wt%).

carbon near the centre area. Therefore, in the as-produced sample (carbon content equals 0.09%), it is likely that the $M_{23}C_6$ carbides tend to form near the surface area where the carbon content is more than 0.07%, and the M_6C carbides tend to form near the centre area where the carbon content is less than 0.07%. As for the tempered sample, carbon becomes more homogenous due to the heat treatment process. It is safe

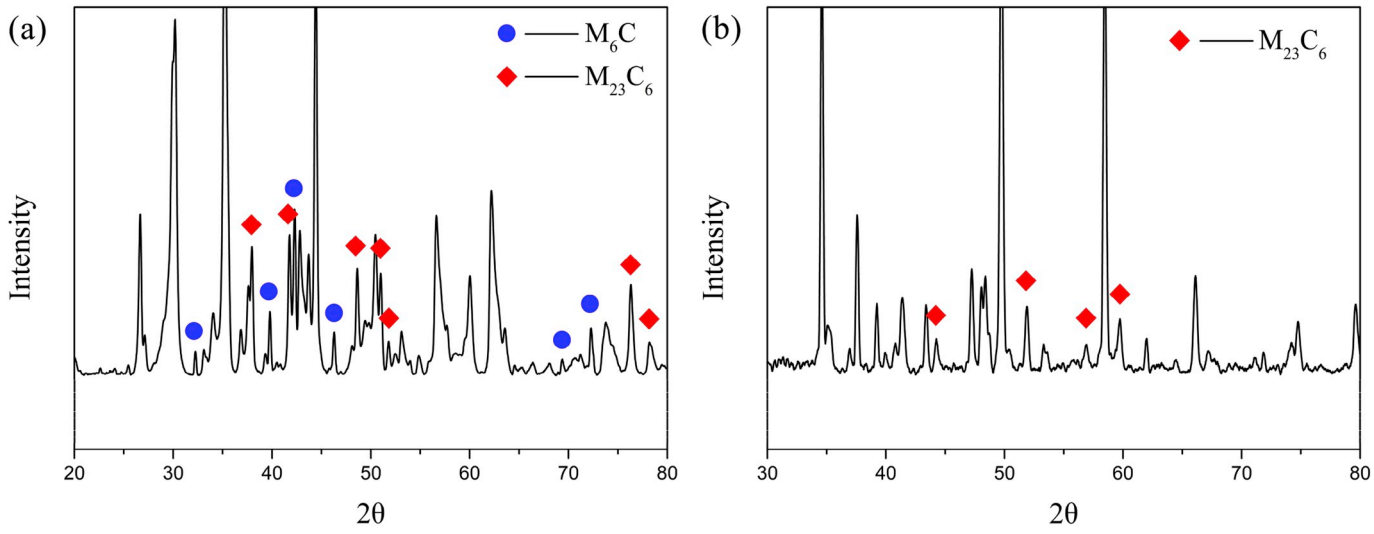

Fig. 7. XRD patterns of the extracted carbides from the (a) as-produced steel and (b) tempered steel.

to assume that the carbon content in the sample is approximately 0.09% on the macroscopic scale. Therefore, only $M_{23}C_6$ carbide would form in the bulk steel at room temperature. Ta carbides and Laves phase predicted by the software were not observed in this study.

TEM images of the microstructure features of the as-produced and tempered steels are shown in Fig. 9. A high density of dislocations is evident in the microstructure of the as-produced steel (Fig. 9a), related to the mechanical alloying process. Meanwhile, homogenously dispersed Y_2O_3 nanoparticles, confirmed by EDS, are observed in the steel matrix (Fig. 9b). Some particles are pinning the dislocation lines, which would lead to an increased creep strength compared to non-ODS steels [29]. The average size of the Y_2O_3 particles in the as-produced steel is 8 nm. The starting size of the Y_2O_3 powder is 25–50 nm, indicating that the mechanical alloying process has a refinement effect on the Y_2O_3 particles. In the tempered steel, dislocation-free areas and martensite laths are observed (Fig. 9c), showing the effect of the normalising and tempering treatment. Fig. 9d shows a dark field image of Y_2O_3 particles pinning the grain boundaries, which is beneficial for enhancing the mechanical properties and extending the working temperature range [30]. The average size of Y_2O_3 is slightly increased to 11 nm after the heat treatment. Fig. 9e and f exhibit the presence of $M_{23}C_6$ carbides along grain boundaries and the diffraction pattern of $M_{23}C_6$, respectively.

3.3. Dislocation density measurement

The dislocation density of the as-produced and tempered steels was calculated from XRD measurements. Assuming that strain broadening is caused by dislocations only, the full width at half maximum (FWHM) of the diffraction profiles can be given by a modified Williamson-Hall plot in quadratic form [31,32]:

$$\Delta K \cong \frac{0.9}{D} + \left(\frac{\pi M^2 b^2}{2}\right)\rho^{\frac{1}{2}}K^2\overline{C} + O\left(K^4\overline{C}^2\right), \tag{1}$$

where ΔK is the full width at half maximum, D is the average grain size, $K = 2sin\theta/\lambda$, θ is the diffraction angle, λ is the wavelength of the X-rays, M is a constant parameter depending on the effective outer cut-off radius of dislocations and is taken as 2 [33], b is the Burgers vector, ρ is the dislocation density and O indicates non-interpreted higher order terms. $\overline{C}$ is an average contrast factor of dislocations and is estimated by Ref. [34]:

$$\overline{C} = \overline{C_{h00}}\left[1 - q\frac{h^2k^2 + h^2l^2 + k^2l^2}{\left(h^2 + k^2 + l^2\right)^2}\right], \tag{2}$$

where $\overline{C_{h00}}$ is the average dislocation contrast factor for the (h00) reflection and is taken as 0.332 [33], q is a parameter that the depends on the elastic constants of the crystal and the edge or screw character of dislocations.

To estimate the dislocation density, equation (1) can be approximated to Ref. [31]:

$$\Delta K^2 \cong \left(\frac{0.9}{D}\right)^2 + \left(\frac{\pi M^2 b^2}{2}\right)\rho K^2\overline{C}. \tag{3}$$

Combining equations (2) and (3), the following relationship can be obtained:

$$\frac{\Delta K^2 - \left(\frac{0.9}{D}\right)^2}{K^2} \cong \left(\frac{\pi M^2 b^2}{2}\right)\rho\overline{C_{h00}}\left[1 - q\frac{h^2k^2 + h^2l^2 + k^2l^2}{\left(h^2 + k^2 + l^2\right)^2}\right]. \tag{4}$$

The dislocation density ρ can therefore be determined by the intercept of equation (4), plotting the left-hand side against the factor which is multiplied by q. The result of the estimated dislocation density of the materials at different conditions is presented in Table 2. As expected, the dislocation density of the normalised steel is significantly increased compared to the as-produced steel due to the martensite transformation. Meanwhile, the dislocation density in the tempered steel is notably lower than the as-produced steel and normalised steel, which can be ascribed to static recovery during the tempering treatment. In the recovery process, the stored energy in the material decreases due to the change in the dislocation structure and growth of the subgrains [35]. Additionally, according to a study of Sandim et al. [36] on the annealing behaviour of ODS Eurofer, dislocation annihilation and/or

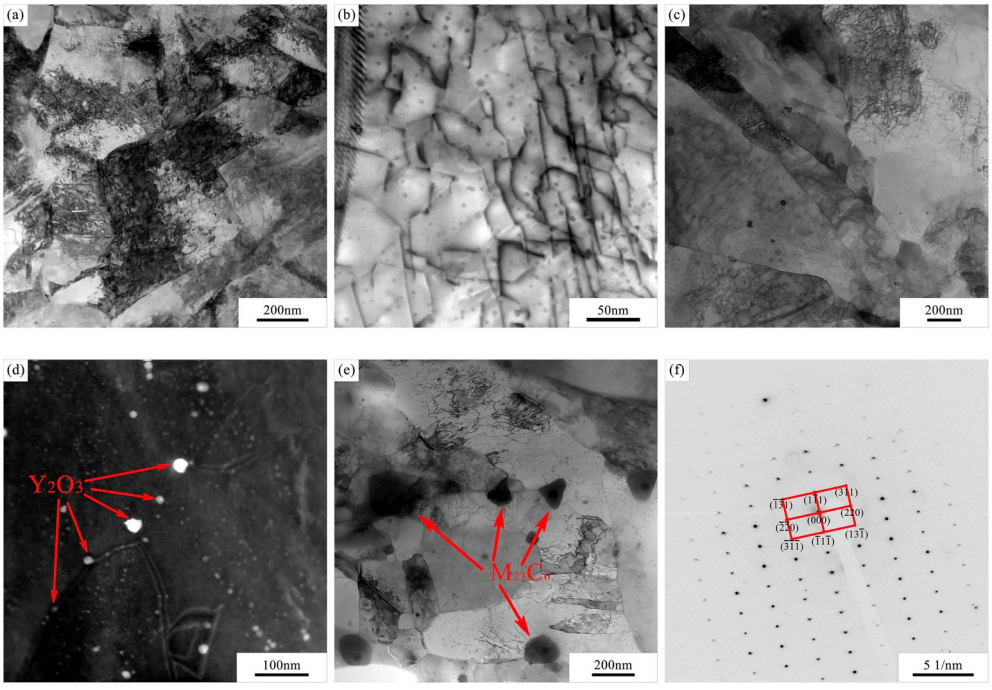

Fig. 9. TEM images of the microstructural features of the (a), (b) as-produced and (c), (d), (e), (f) tempered steel, (a) high density dislocations, (b) homogenously dispersed Y_2O_3, (c) tempered martensite lath and clean grains, (d) Y_2O_3 pinning the grain boundaries (e) $M_{23}C_6$ carbides and (f) diffraction pattern of $M_{23}C_6$ carbides.

Table 2
Dislocation density of the materials at different conditions.

	As-produced steel	Normalised steel (1150 °C)	Tempered steel
Dislocation density/ m^{-2}	2.2×10^{14}	9.4×10^{14}	8.9×10^{13}

rearrangement occurs when the heat treatment temperature is in the ferritic regime, resulting in a decrease in dislocation density.

4. Yield strength modelling

Table 3 shows the tensile properties of the as-produced and tempered steels at room temperature obtained from our previous study. The specimen dimensions and testing method can be found in Ref. [12]. It can be seen that the as-produced steel has a higher tensile strength compared to Eurofer 97 steel (680 MPa) [30] and SPS prepared ODS Fe–9Cr steels (734 MPa) [10], while the tempered steel has a good combination of high strength and a reasonable ductility. From the results of the microstructure characterisation, it is shown that ODS Eurofer consists of steel matrix, precipitates, a bimodal grain size distribution, dislocations and nanoparticles. All of these features contribute to the mechanical properties of the material. To further quantify the contributions of each microstructural component, the following equation is used to estimate the yield strength of the steel at room temperature [37]:

$$\sigma_y = \sigma_0 + \sigma_{ss} + \sigma_{GB} + \left(\sigma_{Dis}^n + \sigma_P^n\right)^{1/n}, \tag{5}$$

where σ_y is the yield strength of the material, σ_0 is friction stress of a single crystal of pure iron, σ_{ss} is the solid solution contribution, σ_{GB} is the grain boundary contribution, σ_{dis} is the forest dislocation hardening contribution, σ_p is the nano-sized oxide particles contribution and n is taken as 2 [37].

σ_{ss} is classically estimated with the following equation:

$$\sigma_{ss} = \sum_i K_i \cdot X_i^z, \tag{6}$$

where K_i a hardening constant, X_i is the atomic fraction of element I, and z equals 0.75 for substitutional solid solution elements i.e. Cr and W [38].

σ_{GB} is usually expressed by the Hall-Petch equation [39,40]:

$$\sigma_{GB} = \frac{k_{GB}}{\sqrt{D}}, \tag{7}$$

where k_{GB} is the Hall-Petch coefficient and D is the mean grain size of the material, as shown in Fig. 4.

σ_{dis} can be described according to Taylor [41] with the following equation:

$$\sigma_{dis} = M\alpha G b\sqrt{\rho}, \tag{8}$$

where M is the Taylor factor that depends on the crystallographic structure and the texture of the material, α is a numerical constant, G is the shear modus for iron, b is the Burgers vector and ρ the dislocation density.

The contribution of nano-sized oxide particles σ_p is estimated by Ashby-Orowan equation [42]:

$$\sigma_p = \frac{0.81MGb}{2\pi(1-\nu)^{1/2}} \frac{ln(2r_s/r_0)}{\lambda - 2r_s} \tag{9}$$

$$\lambda = 2\sqrt{\frac{2}{3}} r \left[\left(\frac{\pi}{4f}\right)^{1/2} - 1\right], \tag{10}$$

where r is the radius of oxide particles, $r_s = 0.816 \times r$ is the mean planar radius of the cross-section of nano-sized oxides, r_0 is the inner cut-off radius of a dislocation core, which is assumed to be the magnitude of the Burgers vector, λ is the average inter-particle spacing, υ is the Possion ratio and f is the volume fraction of nano-sized oxides, which is estimated by the following equation [11]:

$$f = 1.5618 \times 10^{-2} \times (wt.\%\ Y_2O_3). \tag{11}$$

Using the above equations for each strengthening component and the parameters listed in Table 4, the experimentally obtained and theoretically estimated yield strength of the as-produced and tempered steels are presented in Fig. 10. It can be noted that the estimated value of the as-produced steel is in the deviation range of the experimental result, indicating a good agreement. A small deviation between the estimated and experimental values of the tempered steel is found, which may be due to the neglect of the contribution of coarsened carbides. Another possible reason is that, as mentioned in section 3.1, finer grains smaller than 0.29 μm was neglected when calculating the average grain size, which will cause the calculated strength to be slightly lower than the real strength. It is evident that the oxide dispersion strengthening, dislocation strengthening and grain boundary strengthening are the major contributions to the yield strength of the as-produced ODS Eurofer at room temperature. The contributions of nanoparticles, dislocations and grain size are 36%, 22% and 27%, respectively. In the tempered steel, as the dislocation density in the material is decreased considerably, while the average size of the oxide particles and the mean grain size do not change significantly, the contributions of nanoparticles, dislocations and grain size are 37%, 15% and 31%, respectively. The oxide dispersion strengthening and grain boundary strengthening are the dominant strengthening mechanisms in the tempered ODS Eurofer.

5. Conclusions

A heat treatment route was designed for powder metallurgy prepared ODS Eurofer steel. The microstructure and mechanical properties were investigated in detail. The condition of normalising at 1150 °C for 1 h and tempering at 700 °C for 1 h is determined to be a suitable heat treatment route for the as-produced steel to homogenise the microstructure and microhardness. The material has a bimodal grain size distribution and a dual phase microstructure in both as-produced and tempered conditions. The as-produced steel has a higher dislocation density of $2.2 \times 10^{14}\ m^{-2}$, with $M_{23}C_6$ and M_6C carbides in the microstructure. Comparatively, the tempered steel has a lower dislocation density of $8.9 \times 10^{13}\ m^{-2}$, with $M_{23}C_6$ carbides decorating the grain boundaries. High-density Y_2O_3 nanoparticles remain homogenously distributed in the steel matrix after the heat treatment, acting as obstacles for the motion of dislocations and grain boundaries. Oxide dispersion strengthening, dislocation strengthening and grain boundary strengthening are the major contributions to the yield strength of the as-produced ODS Eurofer, while oxide dispersion strengthening and grain boundary strengthening are the dominant strengthening mechanisms in the tempered ODS Eurofer.

Table 3
Tensile properties of the as-produced and tempered ODS Eurofer at room temperature [12].

	Tensile strength/MPa	Yield strength/MPa	Elongation/%	Young's Modulus/GPa
As-produced	1301.2	923.7	6.86	204.1
Tempered	1030.8	861.6	10.4	205.5

Table 4
Parameters used for the yield strength model.

Parameters	σ_0/MPa	K_{Cr}/(MPa·at%$^{-3/4}$)	K_W/(MPa·at%$^{-3/4}$)	k_{GB}/(MPa·μm$^{1/2}$)	M	α	G/GPa	b/nm	υ
Values and references	53.9 [43]	9.95 [44]	75.79 [41]	210 [45]	3.06 [43]	0.38 [43]	81.6 [43]	0.25 [11]	0.334 [43]

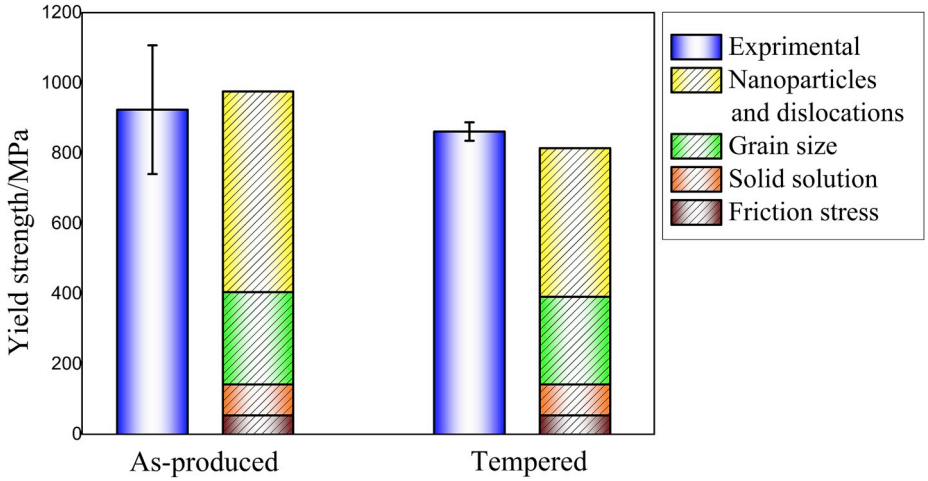

Fig. 10. The experimental and estimated yield strength of the as-produced and tempered ODS Eurofer.

Data availability

The raw/processed data required to reproduce these findings cannot be shared at this time as the data also forms part of an ongoing study.

Acknowledgements

This research was carried out under project number T16010f in the framework of the Partnership Program of the Materials innovation institute M2i (www.m2i.nl) and the Netherlands Organisation for Scientific Research (www.nwo.nl). The authors thank the industrial partner Nuclear Research and Consultancy Group (NRG) in this project for the financial support. The authors also thank Prof. Dr. ir. Roumen Petrov for the help in EBSD analysis and Dr. Vitaliy Bliznuk for the TEM measurement.

References

[1] G. Odette, M. Alinger, B. Wirth, Recent developments in irradiation-resistant steels, Annu. Rev. Mater. Res. 38 (2008) 471–503.
[2] S. Ukai, T. Kaito, S. Ohtsuka, T. Narita, M. Fujiwara, T. Kobayashi, Production and properties of nano-scale oxide dispersion strengthened (ODS) 9Cr martensitic steel claddings, ISIJ Int. 43 (12) (2003) 2038–2045.
[3] S. Ukai, M. Fujiwara, Perspective of ODS alloys application in nuclear environments, J. Nucl. Mater. 307 (2002) 749–757.
[4] C. Suryanarayana, Mechanical alloying and milling, Prog. Mater. Sci. 46 (1–2) (2001) 1–184.
[5] M. Kubota, Properties of nano-structured pure Al produced by mechanical grinding and spark plasma sintering, J. Alloy. Comp. 434 (2007) 294–297.
[6] L. Wang, J. Zhang, W. Jiang, Recent development in reactive synthesis of nanostructured bulk materials by spark plasma sintering, Int. J. Refract. Metals Hard Mater. 39 (2013) 103–112.
[7] M. Suárez, A. Fernández, J. Menéndez, R. Torrecillas, H. Kessel, J. Hennicke, R. Kirchner, T. Kessel, Challenges and Opportunities for Spark Plasma Sintering: a Key Technology for a New Generation of Materials, Sintering Applications, 2013, pp. 320–338.
[8] X. Boulnat, M. Perez, D. Fabregue, T. Douillard, M.H. Mathon, Y.D. Carlan, Microstructure evolution in nano-reinforced ferritic steel processed by mechanical alloying and spark plasma sintering, Metall. Mater. Trans. A 45 (3) (2014) 1485–1497.
[9] S. Noh, A. Kimura, T.K. Kim, Diffusion bonding of 9Cr ODS ferritic/martensitic steel with a phase transformation, Fusion Eng. Des. 89 (7–8) (2014) 1746–1750.
[10] Q.X. Sun, Y. Zhou, Q.F. Fang, R. Gao, T. Zhang, X.P. Wang, Development of 9Cr-ODS ferritic-martensitic steel prepared by chemical reduction and mechanical milling, J. Alloy. Comp. 598 (2014) 243–247.
[11] X. Zhou, Y. Liu, L. Yu, Z. Ma, Q. Guo, H. Yuan, H. Li, Microstructure characteristic and mechanical property of transformable 9Cr-ODS steel fabricated by spark plasma sintering, Mater. Des. 132 (2017) 158–169.
[12] J. Fu, J. Brouwer, I. Richardson, M. Hermans, Effect of mechanical alloying and spark plasma sintering on the microstructure and mechanical properties of ODS Eurofer, Mater. Des. 177 (2019), 107849.
[13] Z. Lu, R.G. Faulkner, N. Riddle, F.D. Martino, K. Yang, Effect of heat treatment on microstructure and hardness of Eurofer 97, Eurofer ODS and T92 steels, J. Nucl. Mater. 386–388 (C) (2009) 445–448.
[14] S.S. Wang, D.L. Peng, L. Chang, X.D. Hui, Enhanced mechanical properties induced by refined heat treatment for 9Cr–0.5Mo–1.8W martensitic heat resistant steel, Mater. Des. 50 (17) (2013) 174–180.
[15] B. Silwal, L. Li, A. Deceuster, B. Griffiths, Effect of postweld heat treatment on the toughness of heat-affected zone for grade 91 steel, Weld. J. 92 (2013) 80–87.
[16] X.L. Wang, C.T. Liu, U. Keiderling, A.D. Stoica, L. Yang, M.K. Miller, C.L. Fu, D. Ma, K. An, Unusual thermal stability of nano-structured ferritic alloys, J. Alloy. Comp. 529 (2012) 96–101.
[17] N. Sallez, X. Boulnat, A. Borbély, J.L. Béchade, D. Fabrègue, M. Perez, Y. de Carlan, L. Hennet, C. Mocuta, D. Thiaudière, Y. Bréchet, In situ characterization of microstructural instabilities: recovery, recrystallization and abnormal growth in nanoreinforced steel powder, Acta Mater. 87 (2015) 377–389.
[18] I. Hilger, F. Bergner, T. Weißgärber, Bimodal grain size distribution of nanostructured ferritic ODS Fe-Cr alloys, J. Am. Ceram. Soc. 98 (11) (2015) 3576–3581.
[19] N. Sallez, P. Donnadieu, E. Courtois-Manara, D. Chassaing, C. Kübel, F. Delabrouille, M. Blat-Yrieix, Y. de Carlan, Y. Bréchet, On ball-milled ODS ferritic steel recrystallization: from as-milled powder particles to consolidated state, J. Mater. Sci. 50 (5) (2015) 2202–2217.
[20] S. Zherebtsov, E. Kudryavtsev, S. Kostjuchenko, S. Malysheva, G. Salishchev, Strength and ductility-related properties of ultrafine grained two-phase titanium alloy produced by warm multiaxial forging, Mater. Sci. Eng., A 536 (2012) 190–196.
[21] C.C. Koch, Optimization of strength and ductility in nanocrystalline and ultrafine grained metals, Scr. Mater. 49 (7) (2003) 657–662.
[22] Y. Wang, M. Chen, F. Zhou, E. Ma, High tensile ductility in a nanostructured metal, ON Nat. 419 (6910) (2002) 912–915.
[23] K.D. Zilnyk, V.B. Oliveira, H.R. Sandim, A. Möslang, D. Raabe, Martensitic transformation in Eurofer-97 and ODS-Eurofer steels: a comparative study, J. Nucl. Mater. 462 (2015) 360–367.
[24] M. Yamamoto, S. Ukai, S. Hayashi, T. Kaito, S. Ohtsuka, Formation of residual ferrite in 9Cr-ODS ferritic steels, Mater. Sci. Eng., A 527 (16) (2010) 4418–4423.
[25] C. Cayron, E. Rath, I. Chu, S. Launois, Microstructural evolution of Y2O3 and MgAl2O4 ODS EUROFER steels during their elaboration by mechanical milling and hot isostatic pressing, J. Nucl. Mater. 335 (1) (2004) 83–102.
[26] M. Taneike, K. Sawada, F. Abe, Effect of carbon concentration on precipitation behavior of M 23 C 6 carbides and MX carbonitrides in martensitic 9Cr steel during heat treatment, Metall. Mater. Trans. A 35 (4) (2004) 1255–1262.
[27] L. Zheng, X. Hu, X. Kang, D. Li, Precipitation of M23C6 and its effect on tensile properties of 0.3C-20Cr-11Mn-1Mo-0.35N steel, Mater. Des. 78 (2015) 42–50.
[28] B. Peng, H. Zhang, J. Hong, J. Gao, H. Zhang, Q. Wang, J. Li, The effect of M 23C 6 on the high-temperature tensile strength of two austenitic heat-resistant steels:

22Cr–25Ni–Mo–Nb–N and 25Cr–20Ni–Nb–N, Mater. Sci. Eng., A 528 (10) (2011) 3625–3629.
[29] M. Ohnuma, J. Suzuki, S. Ohtsuka, S.W. Kim, T. Kaito, M. Inoue, H. Kitazawa, A new method for the quantitative analysis of the scale and composition of nanosized oxide in 9Cr-ODS steel, Acta Mater. 57 (18) (2009) 5571–5581.
[30] R. Lindau, A. Möslang, M. Rieth, M. Klimiankou, E. Materna-Morris, A. Alamo, A.-A. Tavassoli, C. Cayron, A.-M. Lancha, P. Fernandez, Present development status of EUROFER and ODS-EUROFER for application in blanket concepts, Fusion Eng. Des. 75 (2005) 989–996.
[31] T. Ungár, J. Gubicza, P. Hanák, I. Alexandrov, Densities and character of dislocations and size-distribution of subgrains in deformed metals by X-ray diffraction profile analysis, Mater. Sci. Eng., A 319 (2001) 274–278.
[32] Z. Arechabaleta, P. van Liempt, J. Sietsma, Quantification of dislocation structures from anelastic deformation behaviour, Acta Mater. 115 (2016) 314–323.
[33] R.A. Renzetti, H.R.Z. Sandim, R.E. Bolmaro, P.A. Suzuki, A. Möslang, X-ray evaluation of dislocation density in ODS-Eurofer steel, Mater. Sci. Eng., A 534 (2012) 142–146.
[34] T. Ungár, G. Tichy, The effect of dislocation contrast on X-ray line profiles in untextured polycrystals, Phys. Status Solidi 171 (2) (1999) 425–434.
[35] B. Kim, D. Sanmartin, P.E.J. Riveradíazdelcastillo, Modelling recovery kinetics in high-strength martensitic steels, Philos. Mag. Lett. 97 (7) (2017) 280–286.
[36] H.R.Z. Sandim, R.A. Renzetti, A.F. Padilha, D. Raabe, M. Klimenkov, R. Lindau, A. Möslang, Annealing behavior of ferritic–martensitic 9%Cr–ODS–Eurofer steel, Mater. Sci. Eng., A 527 (15) (2010) 3602–3608.
[37] J. Shen, Y. Li, F. Li, H. Yang, Z. Zhao, S. Kano, Y. Matsukawa, Y. Satoh, H. Abe, Microstructural characterization and strengthening mechanisms of a 12Cr-ODS steel, Mater. Sci. Eng., A 673 (2016) 624–632.
[38] P. Susila, D. Sturm, M. Heilmaier, B.S. Murty, V.S. Sarma, Effect of yttria particle size on the microstructure and compression creep properties of nanostructured oxide dispersion strengthened ferritic (Fe–12Cr–2W–0.5Y 2 O 3) alloy, Mater. Sci. Eng., A 528 (13) (2011) 4579–4584.
[39] E.O. Hall, The deformation and ageing of mild steel: III discussion of results, Proc. Phys. Soc. Sect. B 64 (9) (1951) 747–753.
[40] N.J. Petch, The cleavage strength of polycrystals, J. Iron Steel Inst. 174 (1953) 25–28.
[41] G.I. Taylor, The mechanism of plastic deformation of crystals. part I. theoretical, Proc. R. Soc. A 145 (855) (1934) 362–387.
[42] J.W. Martin, Micromechanisms in Particle-Hardened Alloys, Cambridge University, 1980.
[43] F.B. Pickering, Physical Metallurgy and the Design of Steels, Applied Science Publishers, London, 1978.
[44] M. Couvrat, Fabrication d'aciers ODS à haute performance: relation procédé, microstructure, propriétés mécaniques vol. 1, University of Rennes, 2013.
[45] D. Preininger, Effect of particle morphology and microstructure on strength, work-hardening and ductility behaviour of ODS-(7–13)Cr steels, J. Nucl. Mater. 329 (1) (2004) 362–368.